BOREAL ENVIRONMENT RESEARCH 20: 261–282 © 2015
ISSN 1239-6095 (print) ISSN 1797-2469 (online) Helsinki 30 April 2015

Implementation of the CORINE land use classification in the regional climate model REMO

Yao Gao[1)], Stefan Weiher[1)2)], Tiina Markkanen[1)], Joni-Pekka Pietikäinen[1)], Hilppa Gregow[1)], Helena M. Henttonen[3)], Daniela Jacob[4)] and Ari Laaksonen[1)5)]

[1)] *Finnish Meteorological Institute, P.O. Box 503, FI-00101 Helsinki, Finland*
[2)] *Brandenburg Technical University, Postfach 101344, D-03013 Cottbus, Germany*
[3)] *Finnish Forest Research Institute, P.O. Box 18, FI-01301 Vantaa, Finland*
[4)] *Max Planck Institute for Meteorology, Bundesstraße 53, D-20146 Hamburg, Germany; and Climate Service Centre, Fischertwiete 1, D-20095 Hamburg, Germany*
[5)] *University of Eastern Finland, Department of Applied Physics, P.O. Box 1627, FI-70211 Kuopio, Finland*

Received 14 June 2013, final version received 2 Dec. 2013, accepted 26 Nov. 2013

Gao Y., Weiher S., Markkanen T., Pietikäinen J.-P., Gregow H., Henttonen H.M., Jacob D. & Laaksonen A. 2015: Implementation of the CORINE land use classification in the regional climate model REMO. *Boreal Env. Res.* 20: 261–282.

Regional climate models provide an effective way to study the effects of land use changes on regional climate conditions. A precise land cover map is a precondition for land use change studies. We introduce a more realistic high-resolution land cover map, CORINE Land Cover (CLC), to replace the Global Land Cover Characteristics Database (GLCCD), which is used as a standard land cover map in the regional climate model REMO. In this study, present-day climate simulations over northern Europe are performed by using REMO at 18-km resolution with both CLC and GLCCD. Simulated maximum and minimum 2-m air temperatures, diurnal temperature range and precipitation are assessed with the observation-based E-OBS data. The updated CLC enhances the realism of the description of present-day land surface. However, biases from simulated climate conditions to observations are only marginally reduced while more improvements are expected to be achieved by further developments in model physics.

Introduction

Until now, no climate model simulation has been carried out for Fennoscandia to study local and regional effects of land cover changes during the 20th century on climate. A prerequisite for land cover change studies is to use the best information on land cover that is available. The Global Land Cover Characteristics Database (GLCCD; U.S. Geological Survey 2001) land cover map was originally chosen for REMO to be a consistent global dataset. However, the GLCCD land cover map is about 20 years old and lacks accuracy over Finland for present-day climate simulations. For instance, the fraction of peatland in Finland is severely underestimated as 0%, which contrasts with the 8.2% in the 10th (2004–2008) national forest inventory; also Deciduous Conifer Forest, a vegetation type in GLCCD, appears in a large area around Oulu

Editor in charge of this article: Veli-Matti Kerminen

in middle Finland in GLCCD, which is incorrect. Instead, there are peatlands in the same area in CORINE Land Cover (CLC; European Environment Agency 2007); moreover, it is also unrealistic that Narrow Conifers in GLCCD is the dominant vegetation type in the lake area in southern Finland. The real situation is that Conifer Boreal Forest and Mixed Forest prevail around lakes in Finland, as is the case in CLC.

The land surface parameters, such as albedo, roughness length, leaf area index (LAI), which are related to land cover types, affect regional climate conditions (Pielke *et al*. 1998, Nobre *et al*. 2004, Gálos *et al*. 2011). Surface albedo determines how much incoming net surface solar radiation will be reflected back from the land surface. Near-surface wind speed and air turbulences are influenced by surface roughness length, which impacts the exchange of moisture, heat energy and momentum between the surface of earth and the atmosphere (Sud *et al*. 1996, Göttel *et al*. 2008, Bathiany *et al*. 2010). LAI and other vegetation characteristics, for example root depth, influence evapotranspiration (ET) (Nobre *et al*. 2004). Finally, the trends in climate conditions are results of integrations of those non-linear interactions and the initial climate (Pitman *et al*. 2004).

These biogeophysical effects of land cover change in boreal area were recently investigated at stand scale by measurements and at the global scale by models (Bala *et al*. 2007, Betts and Ball 1997, Bathiany *et al*. 2010). A decrease in the local nighttime minimum temperature during the growing season was observed roughly for the first 15 years after the drainage for forestation in Finland (Solantie 1994). The reason for this nocturnal cooling phenomenon is that the dry peat insulates the lower soil layers from the atmosphere. Therefore, the heat flux from a drained peat soil cannot compensate the radiative cooling at the surface which leads to a drop in minimum temperatures (Venäläinen *et al*. 1999). On a longer time scale, the growing forest on formerly open peatlands leads to a decrease in albedo. That is because of the tree cover which is darker in comparison with the grass cover which is lighter during snow-free periods, and the partial snow cover in forested areas as compared with the full snow cover in open areas during snow-cover periods. This increases daily maximum temperatures due to an increase in the absorption of short-wave radiation (Solantie 1994). A consistent result was found by Lohila *et al*. (2010) based on measurements at different drained and undrained peatland sites. Their results show an increase in the April diurnal temperature range (DTR) due to a greater increase in maximum, than in minimum temperatures, possibly as a result of the change in surface radiative properties after drainage. By means of an earth system model, Bathiany *et al*. (2010) also found that afforestation in boreal areas leads to an increase in maximum surface temperature in spring due to albedo changes, and a small increase in annual mean cloud cover, as well as changes in atmospheric circulation due to changes in wind speed and direction. Similarly, Betts (2001) and Bala *et al*. (2007) found that forestation in northern latitudes increases the surface temperatures because the albedo-induced warming typically exceeds the cooling due to the changes in ET and carbon uptake by forests.

In this study, we improved the land use classification over northern Europe in REMO by implementing a more recent dataset of much higher resolution — CLC. In order to get a clear picture of how much the new classification affects the simulation results, we simulated the present-day climate over Fennoscandia. The sensitivity of REMO to two different land cover datasets, the outdated and the new one, were analysed based on two decadal model runs by concentrating on near-surface meteorological variables and land-atmosphere interactions. Furthermore, the observation-based E-OBS data are used as a reference for the simulated maximum and minimum 2-m air temperatures, DTR, as well as precipitation. Similar approaches demonstrated improvements in near-surface temperatures (Yucel 2006, Sertel *et al*. 2010) and significant impacts on local flow patterns (Cheng and Byun 2008). The main goal of this work is to implement a more realistic land use classification map in REMO as a basis for future modelling studies. Only then, regional climate effects of past wetland forestation and of potential forest management strategies in Finland can be analysed with better certainty.

Model description and surface parameter fields

The regional climate model REMO

The regional climate model REMO applied in this study is a three-dimensional hydrostatic atmospheric circulation model. It was developed at the Max-Planck-Institute for Meteorology in Hamburg, Germany. Its dynamical core is based on the former numerical weather prediction model Europa-Modell of the German Weather Service (Majewski 1991). The physical parameterization in REMO follows that of the atmospheric general circulation model ECHAM4 (Roeckner *et al*. 1996), although many physical packages are updated from later version of ECHAM, and adapted to higher resolution. Prognostic variables are surface pressure, temperature, horizontal wind components, specific humidity and cloud liquid water and ice. REMO operates on a rotated horizontal-spherical grid in order to avoid numerical problems caused by the convergence of meridians. Vertically, a hybrid sigma-pressure coordinate system is employed, with the model levels following the terrain near the surface, and progressively approaching pure pressure levels with increasing height. In the eight outermost grid boxes at each lateral boundary, the sponge zone, REMO is relaxed toward the larger scale forcing data with exponentially decreasing influence toward the centre of the domain according to the relaxation scheme of Davies (1976). More detailed information on model characteristics can be obtained from Jacob and Podzun (1997), Jacob (2001) and Jacob *et al*. (2001).

The following gives an overview of the land surface scheme (LSS) used in REMO with respect to the objectives of this study. According to the so-called tile approach, implemented in REMO by Semmler *et al*. (2004), the total surface of each grid box is divided into fractions of land, water and sea ice. Land is further split into fractions of vegetation cover and bare soil. Surface parameters are then calculated separately for each fraction of a grid box and afterwards averaged with their respective areas as weights. Based on data describing the global spatial distribution of land cover types on the land surface, Hagemann *et al*. (1999) and Hagemann (2002) developed parameter values that are assigned to each vegetation type: background surface albedo (albedo over snow-free land areas), roughness length, fraction of green vegetation cover, LAI (ratio of one-sided leaf area to ground area), forest ratio (ratio of trees regardless of their photosynthetic activity), soil water holding capacity (maximum amount of water that plants may extract from the soil before wilting begins) and volumetric wilting point (percentage of moisture in a soil column below which plants start to wilt).

LAI, fractional green vegetation cover and background surface albedo undergo pronounced seasonal variability. The intra-annual cycle of vegetation phenology without interannual variation was introduced to REMO by Hagemann (2002). Therein, the seasonal cycles of LAI and fractional green vegetation cover are derived from a monthly varying growth factor that determines the growth characteristics of the vegetation in conjunction with minimum and maximum values of LAI and fractional green vegetation cover referring to dormancy and growing season, respectively. The growth factor in turn is calculated from the fraction of photosynthetically active radiation for latitudes between 40°N and 40°S, and from a 2-m temperature climatology (Legates and Willmott 1990) for higher latitudes. In REMO, the evaporation that takes place above the vegetation surface is related to the wet skin fraction, which describes the ability to store precipitation water and is calculated through the fractional green vegetation cover and LAI; however, when the wet skin is dry, LAI takes part in the calculation of stomatal resistance as a factor for the aim to get transpiration amount (Preuschmann 2012). Background surface albedo is a function of monthly varying LAI. During the snow cover period, surface albedo is a function of snow albedo, background surface albedo and snow depth, in which snow albedo depends on snow surface temperature and forest ratio in REMO (Kotlarski 2007). In a later step, the seasonal cycle of surface albedo was improved (Rechid 2008, Rechid *et al*. 2009). They implemented an advanced parameteriza-

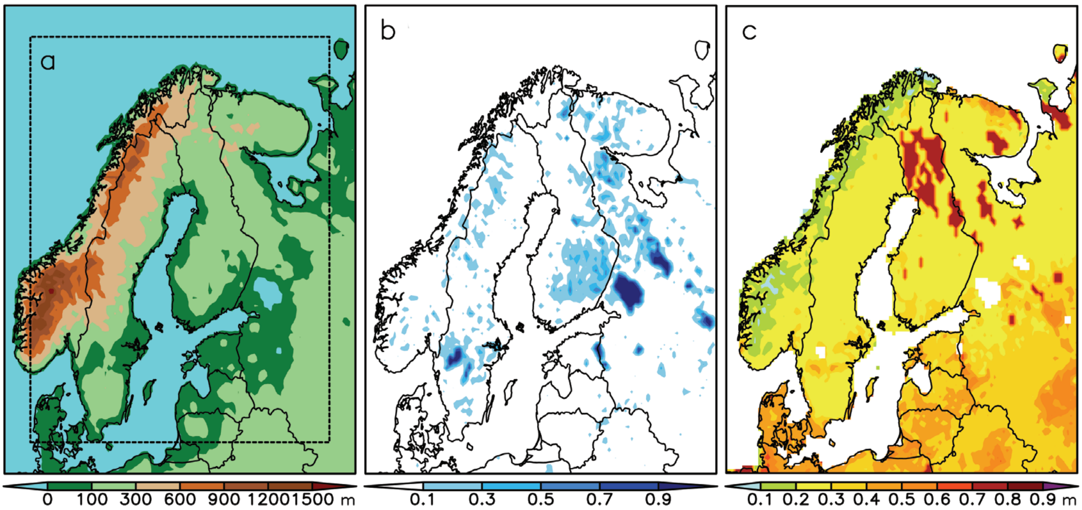

Fig. 1. (**a**) Orography, (**b**) inland water fraction, and (**c**) field capacity in the CLC surface library. The dashed frame in **a** shows the extent of the relaxation zone, i.e. the eight outer most grid boxes in each direction.

tion of snow-free land surface albedo as a function of vegetation phenology. For this, they used MODIS satellite data from a period 2001–2004 in order to derive global distributions of pure soil and vegetation albedo which in turn are used together with monthly varying LAI to compute annual background surface albedo cycles.

In addition, heat diffusion equations are solved for the five soil layers with a zero-heat-flux condition applied at the bottom near ten meters depth. Heat conductivity and heat capacity are dependent on the soil type (Kotlarski 2007). Changes in the aggregate state of water within the soil, leading to release and absorption of latent heat, were introduced by Semmler (2002).

REMO's soil hydrology is parameterized via water budget equations for three different reservoirs: snow cover, skin reservoir (water by vegetation interception) and soil (Rechid 2009). A bucket-like soil moisture reservoir is filled by precipitation and snow melt and depleted via evaporation from the upper ten centimetres of bare soil. From below, the soil water storage is emptied via transpiration from the vegetation and subsurface drainage. Surface runoff will occur in case the soil moisture content reaches saturation.

For a more detailed description of the LSS, the interested reader is referred to Kotlarski (2007) and Rechid (2009).

Study area and land cover data

Our study area focuses on Fennoscandia, with the modelling domain being centred around Finland. The area encompasses a region of roughly 52°–72°N and 4°–40°E. This region is characterized by mostly flat land with model topography not rising higher than 300 m (Fig. 1a). An exception to this is the Scandinavian mountain range, the Scandes, stretching along the border between Sweden and Norway. Furthermore, Fennoscandian countries are surrounded by the North Atlantic Ocean and the large water body of the Baltic Sea. Inland water fractions are also high, especially in southern and middle Finland as well as in parts of Russia that are near to the east of Finland (Fig. 1b).

For the derivation of the surface parameter fields in REMO, a description of the land cover is necessary. The standard global dataset of major ecosystem types employed in REMO is GLCCD, constructed according to classifications of Olson (1994a, 1994b). Based on AVHRR satellite data from a period covering April 1992 to March 1993, the U.S. Geological Survey constructed a dataset displaying the global distribution of 78 Olson ecosystem types at 1-km horizontal resolution (Loveland *et al*. 2000). For in-depth information on the current GLCCD, *see* U.S. Geological Survey (2001).

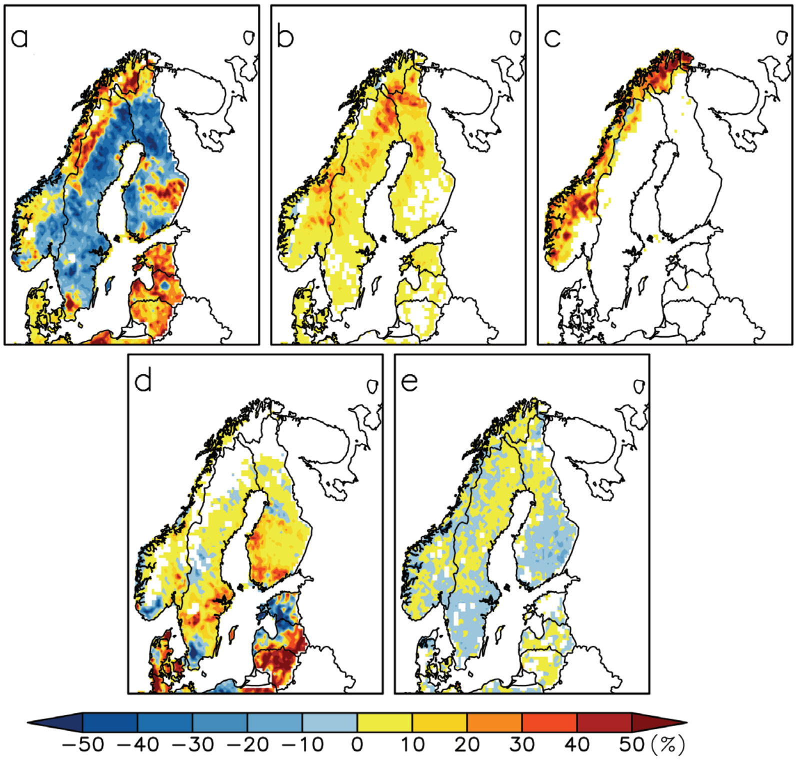

Fig. 2. Changes (%) [(CLC – GLCCD) × 100%/GLCCD] in fractional coverage for the land cover groups: (**a**) forests, (**b**) wetlands, (**c**) barren lands, (**d**) agricultural areas, and (**e**) inland water.

In order to obtain a more accurate and up-to-date representation of land cover for regional modelling purposes, CLC data on a European scale is used in this study. CLC has a horizontal resolution of 100 m and comprises 44 different land cover classes. Based on images from two satellites from a 2006 ± 1 year period measured with the HRVIR and LISS III instruments, a depiction of the current European vegetation coverage was derived (European Environment Agency 2007).

Because of the limited spatial extent of CLC data, the modelling domain is not entirely covered. CLC does not cover Russia and Belarus, and for this part of the model domain, GLCCD data are used in both simulations. No matter whether such a merging is needed or not, the problem of matching vegetation classes of both data sets lies at hand. In order to make use of the existing parameter allocations, corresponding to vegetation types in GLCCD, translations of the vegetation types between CLC and GLCCD were derived (Table 1). In a first approach the matching was performed by subjectively comparing definitions and photographs given in EIONET (http://sia.eionet.europa.eu/CLC2000/classes) and Olson (1994a) for CLC and GLCCD, respectively. For some classes finding an appropriate analogue was rather straightforward: for example matching Broad-leaved Forest, Coniferous Forest and Mixed Forest from CLC with Cool Broadleaved Forest, Conifer Boreal Forest and Cool Mixed Forest from GLCCD, respectively. However, for some classes, e.g. Transitional Woodland/Shrub, a similar GLCCD class was not obvious. Despite a certain degree of subjectiveness, we consider this translation method to be appropriate in this study.

To depict changes in the spatial distribution of land cover types when employing CLC, similar classes were joined together in groups according to the land cover classification in GLCCD: (1) Forests (Conifer Boreal Forest, Cool Mixed Forest, Cool Broadleaved Forest and Deciduous Conifer Forest), (2) Wetlands (‘Mire, Bog, Fen’ and Marsh Wetlands), (3) Barren lands (Barren Tundra and Polar Alpine Desert), (4) Agricultural areas (‘Cool Grasses and Shrubs’, ‘Cool Fields and Woods’, ‘Grass Crops’ and ‘Crops, Grass, Shrubs’) and (5) Inland water. The differences between the two land cover maps are displayed for each group (Fig. 2) and changes in fractional coverage (excluding sea water grid points) are summarized (Table 2). In most parts of Finland and Sweden, the coverage with forest types (Fig. 2a) is higher in GLCCD than that in CLC, which is mostly due to a decrease in the extent of Conifer Boreal Forest in CLC and

Table 1. Vegetation types of CLC and their translations into GLCCD classes.

	CLC types		GLCCD types
Artificial areas			
1	Continuous urban fabric	1	Urban
2	Discontinuous urban fabric	30	Cool crops and towns
3	Industrial or commercial units	1	Urban
4	Road and rail networks and associated land	1	Urban
5	Port areas	1	Urban
6	Airports	30	Cool crops and towns
7	Mineral extraction sites	1	Urban
8	Dump sites	1	Urban
9	Construction sites	1	Urban
10	Green urban areas	25	Cool broadleaved forest
11	Sport and leisure facilities	30	Cool crops and towns
	Agricultural areas		
12	Non-irrigated arable land	93	Grass crops
13	Permanently irrigated land*	–	–
14	Rice fields*	–	–
15	Vineyard*	–	–
16	Fruit trees and berry plantations	94	Crops, grass, shrubs
17	Olive groves*	–	–
18	Pastures	40	Cool grasses and shrubs
19	Annual crops associated with permanent crops*	–	–
20	Complex cultivation patterns	93	Grass crops
21	Land principally occupied by agriculture, with significant areas of natural vegetation	55	Cool fields and woods
22	Agro-forestry areas*	–	–
Forest and semi-natural areas			
23	Broadleaved forest	25	Cool broadleaved forest
24	Coniferous forest	21	Conifer boreal forest
25	Mixed forest	23	Cool mixed forest
26	Natural grassland	42	Cold grassland
27	Moors and heathland	64	Heath scrub
28	Sclerophylous vegetation	64	Heath scrub
29	Transitional woodland/shrub	62	Narrow conifers
30	Beaches, dunes and sand plains	50	Sand deserts
31	Bare rock	69	Polar alpine desert
32	Sparsely vegetated areas	53	Barren tundra
33	Burnt areas**	21	Conifer boreal forest
34	Glaciers and perpetual snow	12	Glacier ice
Wetlands			
35	Inland marshes	45	Marsh wetland
36	Peatbogs	44	Mire, bog, fen
37	Salt marshes	45	Marsh wetland
38	Salines*	–	–
39	Intertidal flats	50	Sand deserts
Waterbodies			
40	Water courses	14	Inland water
41	Water bodies	14	Inland water
42	Coastal lagoons	14	Inland water
43	Estuaries	14	Inland water
44	Sea and ocean	15	Sea water

* CLC classes that do not exist in the modelling domain used in this study.
** There is no appropriate analogue for Burnt areas in GLCCD. Because this type mostly occurs in Sweden it was decided to preliminarily translate it to a forest type, Conifer Boreal Forest, which is most common in this area.

the misrepresentation of peatlands as Deciduous Conifer Forest in middle Finland in GLCCD (not shown). On the other hand, the representation of Cool Broadleaved Forest in northern Finland and Norway and the occurrence of Cool Mixed Forest in the Baltic States are higher in CLC. Wetlands (Fig. 2b) are vastly underrepresented in GLCCD in most of the area considered, leading to an increase of 2.7%. The percentage of Barren lands (Fig. 2c) is higher by 2.5% in CLC implying that sparsely- or non-vegetated regions are actually more vegetated in GLCCD. Also, in CLC the coverage of Agricultural areas (Fig. 2d) is higher than in GLCCD. The most prominent anomalies are located in southern Sweden and in Estonia, where forests take up more space in CLC. The higher resolution of CLC data allows for a better representation of small lakes (Fig. 2e), which are plentiful in Fennoscandia. However, this higher resolution is also responsible for a more accurate description of the lake shores and thus their extent which, in comparison to GLCCD, leads to an overall decrease in the spatial coverage of Inland water by 0.6%. The decreases in lake fractions are most noticeable in the lake area of southern Finland.

Development of surface parameter fields for REMO

The surface parameter fields of REMO are collected into the so-called surface library which includes the following datasets: a topography map, a soil texture map, an annual mean vegetation albedo map, an annual mean soil albedo map, a map of growth factors, a land cover map and the parameter values assigned to each land cover type. For this study, two different sets of surface libraries were constructed due to the different land cover descriptions of CLC and GLCCD. While LAI, fractional green vegetation cover and background surface albedo have intra-annual cycles, all other fields are constant throughout a model simulation. The contents of a surface library are summarized (Table 3).

Orography and variance of the orography are derived from the U.S. Geological Survey's GTOPO30 dataset (USGS GTOPO30) with a horizontal resolution of 30 arc seconds or approximately one kilometre. The distribution of soil texture types stems from Zobler (1986) and is based on soil data from FAO/UNESCO (1971–1981). These three parameter fields are the only fields that are identical for both surface libraries.

The land-sea mask is constructed according to the land-sea/lake distribution in the respective land cover maps. The forest ratio and the field capacity of soil are constructed by allocating their respective parameter values to the land cover types in the resolution of the respective land cover map. In the next step, they are aggregated to the coarser REMO resolution by linearly averaging all values per REMO grid box weighted by the fractional area of each represented land cover type (Hagemann *et al*. 1999).

However, as described in Claussen *et al*. (1994), linear averaging is not valid for roughness length. The aggregation of an average roughness length to a REMO grid box is done by logarithmically averaging land cover type specific drag coefficients at a so-called blending height. After Mason (1988), this is a certain height for turbulent flow above a heterogeneously vegetated surface at which the influences of individual surface patches on vertical profiles or fluxes become horizontally blended. REMO uses 100 meters as the standard blending height. The total roughness length as part of the sur-

Table 2. Fractional coverage (%) of specified land cover groups (CLC translated to GLCCD, *see* Table 1) over land area, i.e. all grid points that are not entirely covered by sea water in the study domain. The change is calculated as CLC – GLCCD.

	Forests	Wetlands	Barren lands	Agricultural areas	Inland water	Rest
GLCCD	38.5	0.1	1.5	9.1	6.7	44.1
CLC	37.3	2.8	4.0	12.2	6.1	37.6
Change	–1.2	+2.7	+2.5	+3.1	–0.6	–6.5

face parameter fields is calculated according to Tibaldi and Geleyn (1981) as the square root of the sum of the squares of roughness length due to variance of the orography and roughness length due to vegetation.

The field capacity is calculated based on the aggregation of plant-available soil water holding capacities and volumetric wilting points. An additional masking according to the spatial distribution of a certain soil type from the FAO/UNESCO (1971–1981) data is applied: especially in northern and middle Finland, the field capacity is widely increased to values of 0.71 m in both surface libraries used in this study (Fig. 1c). According to the FAO (http://www.fao.org/ag/AGL/agll/prosoil/histo.htm), this area is associated with the soil type Histosol which is characterized, among other things, by its content of organic matter (peat) and wet soil conditions.

Subgrid-scale variability of soil water capacities within a model grid box is accounted for by an improved surface runoff parameterization scheme (Hagemann and Gates 2003) based on the Arno scheme developed by Dümenil and Todini (1992). The resulting surface parameter fields in this respect are denoted b, W_{min} and W_{max}. In the improved scheme the shape parameter b does not depend anymore solely on subgrid topographic variability but also on soil water capacity heterogeneity with regard to soil type and vegetation. W_{min} and W_{max} are the subgrid minimum and maximum, respectively, soil water capacities. These three parameters are calculated for a subgrid scale of 1/10 of the REMO horizontal resolution.

Table 3. Surface parameter fields that are used in REMO, either constant in time or as annual cycles.

	Parameter (unit)
Identical for both surface-parameter fields (constant in time)	
1	Orography (m)
2	Variance of the orography (m^2)
3	Soil texture types
Different for both surface-parameter fields (constant in time)	
4	Land sea mask
5	Total roughness length (m)
6	Forest ratio
7	Field capacity of soil (m)
8	b
9	W_{min} (m)
10	W_{max} (m)
Different for both surface-parameter fields (annual cycles)	
11	Background surface albedo (i.e. surface albedo over snow free area)
12	Fractional green vegetation cover
13	Leaf area index

The seasonal cycles of background surface albedo, LAI and fractional green vegetation cover for each vegetation type are aggregated to the REMO grid by linear averaging. For Conifer Boreal Forest, the fractional green vegetation cover in the dormancy and growing seasons and the forest ratio are given in Hagemann (2002) to be 0.52, 0.52 and 0.46, respectively. In the simulation based on GLCCD in this study, for Fennoscandia these values are increased to the values proposed by Claussen *et al*. (1994), i.e. 0.91, 0.91 and 0.8, respectively. In the case of CLC, however, the values are set to those given in Hagemann (2002) because they compare better to measurements and analyses by the Finnish Environment Institute (P. Härmä, Finnish Environment Institute, and S. Hagemann, MPI for Meteorology, pers. comm.). It is assumed that this also holds for Conifer Boreal Forest in parts of the modelling domain outside Finland.

Generally, most of the CLC surface library fields only differ with GLCCD surface library fields in regions where CLC data is available. Exceptions are the identical fields and those affected by the described changes regarding Conifer Boreal Forest.

Experiment setup and evaluation data

Experiment setup

In order to study the sensitivity of REMO to two different sets of surface parameter fields, two decadal model runs were performed with REMO. The runs were forced every six hours by meteorological boundary data from ECMWF ERA-Interim reanalysis data (Simmons *et al*. 2007). Sea surface temperature and sea ice distribution were taken from ERA-Interim as well. The initial conditions for the REMO runs and the greenhouse gas concentrations were identical. The modelled period encompasses 1 January 2000 until 31 December 2009 for a domain covering Fennoscandia (Fig. 1). The horizontal resolution for the grid, consisting of 109 × 121 grid boxes, is 0.167° which is approximately 18 km. In the vertical, 27 atmospheric layers are used reaching about 25 km at the centre of the top atmospheric layer with a top-of-the-atmosphere pressure of 0 hPa. To derive the uncertainties from internal model variability requires ensemble model simulations, but we consider that the uncertainties from internal model variability of the model runs is low in this study because the size of model domain is small and the influence from lateral boundary forcing is strong (Aldrian *et al*. 2004).

In both model runs, surface and soil fields (soil, snow and surface temperatures, specific humidity, soil wetness, snow depth and skin reservoir content) were initialized by using the corresponding fields from a 0.44° REMO model simulation started in 1989 and covering the whole European area interpolated to the finer resolution. Because of this warm start, soil heat fluxes were expected to be in a near-equilibrium state which should minimize effects on simulated surface temperatures and surface fluxes. However, looking at the temporal evolution of monthly area mean temperatures in all five soil layers, the lowest two soil layers did not reach an equilibrium state in some areas until the end of the simulation. This means that there is still a heat flux into the soil throughout the model run. Because this affects both model runs to a similar degree and the influence of the deep-soil temperature on the surface soil temperature is expected to be small, we consider this to be an acceptable initialization in this study. The first simulated year was excluded from the analysis to allow for the model to adapt to the individual atmosphere and soil conditions according to the different surface parameter fields. Therefore, all following results are only based on the nine-year period of 2001–2009.

For simplicity the REMO model run based on GLCCD land cover will be referred to as $GLCCD_{sim}$ and the model run that used CLC will be called CLC_{sim} from here on.

Evaluation data

For comparison of simulation results with observations, the E-OBS dataset (version 7.0; http://www.ecad.eu/download/ensembles/download.php) on a 0.22° rotated grid is applied. E-OBS is used for evaluating mean monthly/seasonal precipitation as well as mean monthly/seasonal 2-m air temperature and DTR. The latter is computed as daily maximum minus daily minimum 2-m air temperature. According to Haylock *et al*. (2008) the maximum (minimum) 2-m air temperature for a specific day is the maximum (minimum) 2-m air temperature measured within the 24-hour period preceding 1800 UTC of that day. To be consistent with observation data the same period is used for model output data. When computing temperature differences between model output and E-OBS data, the simulated temperature is height-corrected to the E-OBS orography by assuming a constant tropospheric lapse rate of 0.0064 K m^{-1}. Afterwards, the height-corrected temperature data is bicubically interpolated to the E-OBS grid, neglecting the REMO relaxation zone. Simulated precipitation is conservatively remapped to the E-OBS grid without taking orography differences into account.

Multi-year monthly means are computed for the period of 1 January 2001 to 31 December 2009. In contrast, multi-year seasonal means use model output and evaluation data from the period of 1 December 2000 to 30 November 2009, thus taking whole winter seasons into account for a nine-year average. The dormancy season in the Northern Europe domain refers to the months from November to April, while the growing season is from May to October.

Results and discussion

Differences between selected surface parameter fields

Differences in surface parameter fields are shown (Fig. 3) for surface library fields without intra-annual cycle: total roughness length, forest ratio and field capacity. To better depict changes in the seasonal cycles of background surface albedo, LAI and fractional green vegetation

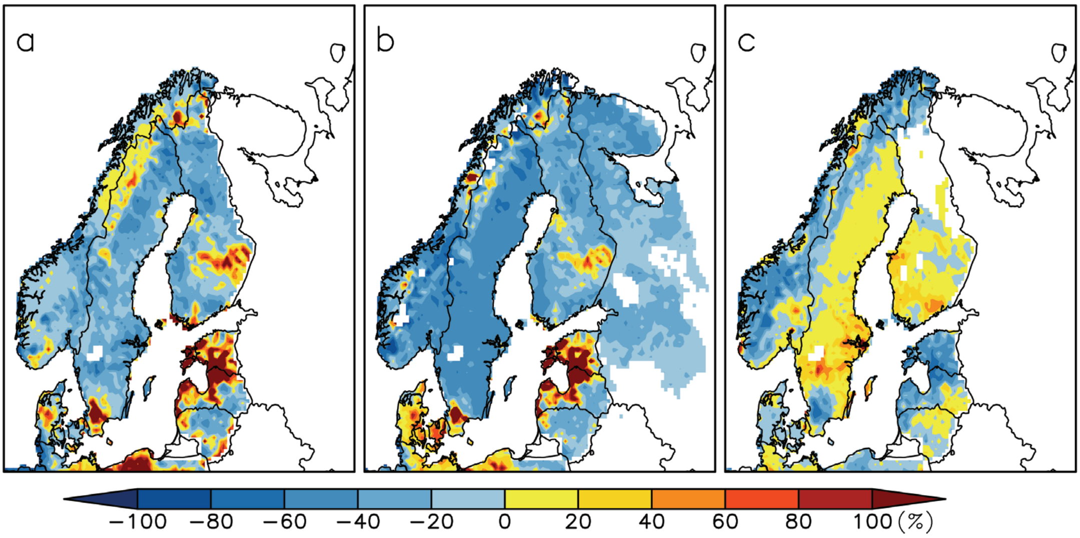

Fig. 3. Percentage changes [(CLC – GLCCD) × 100%/GLCCD] for surface library fields without intra-annual cycle: (**a**) total roughness length, (**b**) forest ratio, and (**c**) field capacity.

cover, monthly and seasonal means are displayed for these parameters (Fig. 4).

Changes in total roughness length (Fig. 3a) are only due to changes in land cover since the underlying orography is identical for both libraries. The change in domain averaged roughness length is –9.73% when employing CLC instead of GLCCD. This is mostly due to changes in the fractional coverage of forests: in large parts of Sweden and Finland, Conifer Boreal Forest is partly exchanged with Narrow Conifers and Wetlands which both have much lower roughness lengths. In contrast, in the lake area of southern Finland, forests are more prominent in CLC and thus lead to an increase of roughness length there.

The differences in forest ratio (Fig. 3b) are dominated mainly by changes in forest coverage, resulting in an overall change of –24.10%. Especially in Finland, the differences are not as high as in Sweden because of two counter acting effects: firstly, a decreased fractional coverage of Conifer Boreal Forest together with a decreased parameter value of forest ratio of it from 0.8 to 0.46; secondly, an increased coverage of Cool Broadleaved Forest and Cool Mixed Forest which has forest ratio of about double of that of Conifer Boreal Forest. Moreover, the forest ratio is higher in the lake area of southern Finland and in parts of Estonia and Latvia in the CLC-based library due to a higher fraction of forests instead of agricultural vegetation types. Although there is no CLC data available for Russia, the forest ratio in the Russian part of the modelling domain is nevertheless influenced by the adjustment of the parameter value of forest ratio for Conifer Boreal Forest, which leads to a decrease in this region.

The overall change of field capacity with respect to GLCCD is –6.16%, which is –13 mm by averaging over the whole model domain. Field capacity differences (Fig. 3c) are most pronounced over the Scandinavian mountain range as well as parts of southern Sweden and northern Estonia and Latvia, with lower values in the CLC-based library. Because of a higher fractional cover of bare and sparsely vegetated areas of the Scandes in CLC, the field capacity is accordingly lower. The much lower values are presented in the very south of Sweden and the north of Baltic States. It is because the GLCCD type 'Crops, Grass, Shrubs' with plant-available soil water holding capacities of 490 mm and volumetric wilting point of 465 mm is mainly replaced by CLC forest types which have much lower plant-available water holding capacities but a similar volumetric wilting point. In contrast, the field capacity is higher in the part with increased agriculture area in Sweden and Finland

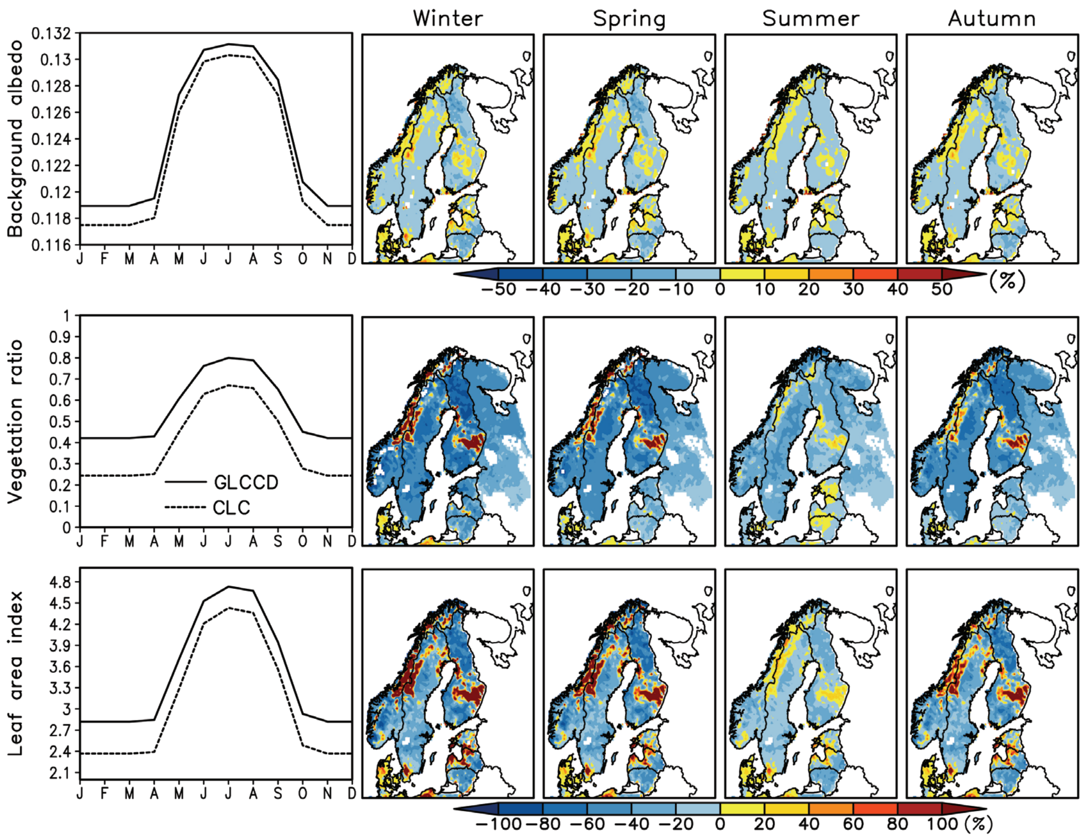

Fig. 4. Differences between surface library fields with intra-annual cycle: background surface albedo (upper row), fractional green vegetation cover (middle row) and leaf area index (lower row). The four rightmost columns show the spatial distribution of percentage changes [(CLC – GLCCD) × 100%/GLCCD] of seasonal averages for all four seasons: spring (MAM), summer (JJA), autumn (SON) and winter (DJF). The leftmost column shows the seasonal cycles of the respective parameters averaged over all land grid points of the domain (as shown to the right) for the two surface libraries GLCCD (solid line) and CLC (dashed line).

(Fig. 2d). In parts of northern and middle Finland, the field fields do not differ at all because of the same masking value is applied regardless of the underlying land cover (Fig. 1c).

The seasonal cycles of fractional green vegetation cover and LAI demonstrate the long dormancy period of vegetation which is about half a year in northern European latitudes (Fig. 4). Differences in the growing season are less pronounced than that during the dormancy season. The main reasons for this are twofold: firstly, the fractional cover with Conifer Boreal Forest decreases, making room for deciduous vegetation types having smaller fractional green vegetation cover in winter. During summer, however, a higher fractional coverage of deciduous species, e.g. Cool Broadleaved Forest and Cool Mixed Forest in CLC, leads to a smaller difference in monthly mean fractional green vegetation ratio and in LAI; secondly, Conifer Boreal Forest is affected by a decreased parameter value of fractional green vegetation cover from 0.91 to 0.52 leading to a further decrease in vegetation fraction, which also happens in parts of Russia. Smaller patches of increases of fractional green vegetation cover and LAI in CLC are attributed to increases in forest coverage instead of agricultural or shrub areas (e.g. Baltic states and southern Sweden), or are associated with increased scrub vegetation in an otherwise sparsely or non-vegetated region (e.g. in some parts of the Scandes).

Because the seasonal cycle of LAI is taken into account in computing seasonal variability

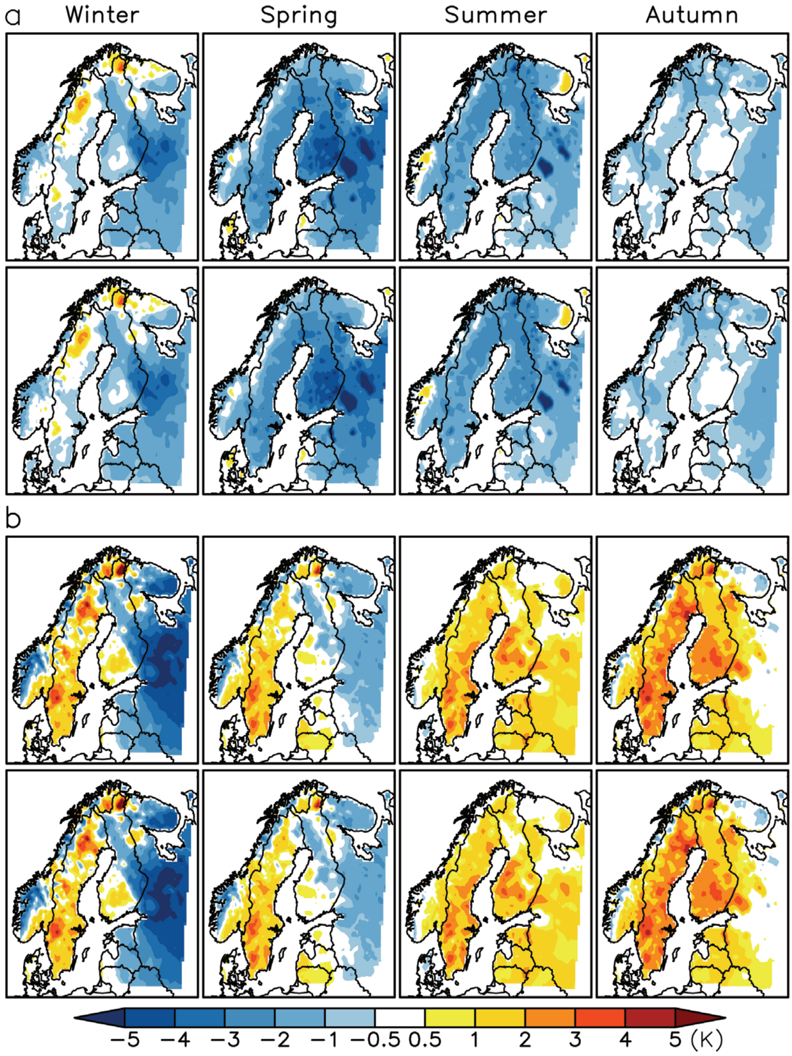

Fig. 5. (**a**) Multi-year seasonal mean differences (REMO – E-OBS) of daily maximum 2-m air temperature (K) in GLCCD simulation (upper row) and in CLC simulation (lower row). (**b**) As upper panel but for daily minimum 2-m air temperature (K).

of background surface albedo (Fig. 4), the background surface albedo increases in places where LAI in CLC is higher than that in GLCCD. In contrast, the background surface albedo in wetland, agricultural and sparsely vegetated areas, such as northern Finland, Lithuania and southern Norway, is lower in the CLC-based surface library. However, it has to be kept in mind that differences between winter and summer are small for the snow-free background surface albedo while they become much more pronounced in the presence of snow.

Two-meter air temperature and precipitation

Temperature

In general, the 2-m air temperatures in the two simulations show similar biases (Fig. 5). The simulated daily maximum 2-m air temperature ($T_{max,2m}$) over land indicate cold biases compared to the E-OBS data throughout the domain with the exception of the positive biases of 1–2 K in Scandinavian mountains in winter. Additionally, the simulated daily minimum 2-m air temperature ($T_{min,2m}$) over land presents warm biases of

1–4 K in summer and autumn in most areas of the model domain, whereas during spring and winter the geographical differences are more pronounced showing the cold biases over Russia and the Baltic countries and warm biases over Sweden. The underestimation of $T_{\mathrm{min,2m}}$ in middle to north of Finland seems to originate from the cold bias above Russia which is more than –5 K in winter. Similar cold biases are also found in eastern Europe for $T_{\mathrm{mean,2m}}$ in REMO simulations in comparison to observation data from the Climate Research Unit (CRU; http://www.cru.uea.ac.uk) but the reason for this is still unclear (Pietikäinen *et al*. 2012).

Several extraordinary spots which appear in these difference maps of both daily $T_{\mathrm{max,2m}}$ and daily $T_{\mathrm{min,2m}}$ are mostly recognized as inland lakes, such as Lake Inari in northern Finland, Lake Orebro in southern Sweden and Lake Ladoga and Lake Onega in Russia. These anomalies are caused by the fact that REMO uses the nearest sea surface temperatures as the lake surface temperatures: Baltic Sea in the case of the two big lakes in Russia and lakes in southern Sweden and southern Finland, and the Arctic sea in the case of Lake Inari. The lakes in Finland and Sweden are relatively small and shallow, thus the daily and seasonal surface temperature changes above those lakes are damped and delayed in REMO simulations as compared with E-OBS data. The too high lake surface temperatures in both $T_{\mathrm{max,2m}}$ and $T_{\mathrm{min,2m}}$ of Lake Inari and Lake Orebro in winter can be observed, however, the $T_{\mathrm{max,2m}}$ is too low but $T_{\mathrm{min,2m}}$ is too high above those lakes in other seasons in the REMO simulations as compared with E-OBS. The features of the surface temperature of the two lakes in Russia should be more similar to those of the Baltic Sea because these two lakes are large and also the Baltic Sea is almost a closed basin. Nevertheless, large anomalies can still be seen above these two lakes especially for $T_{\mathrm{max,2m}}$. The reason for this may be that the gridded E-OBS temperature data is derived from land stations only and that temperatures of those lake grid points, especially for such big lakes as Ladoga and Onega, might not be well captured by the used interpolation algorithm.

The widespread underestimation of $T_{\mathrm{max,2m}}$ and overestimation of $T_{\mathrm{min,2m}}$ causes a too low DTR in all seasons (Fig. 6). Compared with other seasons, winter is the season that the modelled DTR matches best with the DTR pattern of E-OBS in magnitude, especially the high winter DTR in Lapland. The reasons can be attributed to two phenomena: firstly, advection of much warmer or much colder air from the North Atlantic within a day's time; secondly, large temperature drops can occur in case of sudden changes from cloudy to cloudless conditions. High amplitudes of DTRs can be seen in the area east of the Scandes to the west of Finland. Foehn effect is most likely to be the main reason for this. Besides, the drained peatlands where forestation did not succeed in western Finland should present bigger DTRs because no trees can counteract the effects caused by the changes in soil properties (Venäläinen *et al*. 1999). Moreover, the DTRs of lake surface temperatures are clearly smaller than the DTRs in surrounding land areas.

In general, the differences in surface temperature between the $\mathrm{CLC_{sim}}$ and $\mathrm{GLCCD_{sim}}$ are difficult to judge gridpoint-wise. According to the monthly areal averaged differences (REMO – E-OBS) (Fig. 7a), the daily $T_{\mathrm{max,2m}}$ and daily $T_{\mathrm{min,2m}}$ in $\mathrm{CLC_{sim}}$ show an improvement in $T_{\mathrm{max,2m}}$, but also an increased overestimation of $T_{\mathrm{min,2m}}$ in the growing season. In the dormancy season, the monthly areal averaged daily $T_{\mathrm{max,2m}}$ and $\mathrm{T_{min,2m}}$ in $\mathrm{CLC_{sim}}$ are lower than those in $\mathrm{GLCCD_{sim}}$. This leads to increased underestimations for both $T_{\mathrm{max,2m}}$ and $T_{\mathrm{min,2m}}$ in REMO, except for the $T_{\mathrm{min,2m}}$ in November which is originally overestimated. The DTR is slightly improved in $\mathrm{CLC_{sim}}$ by less than 0.2 K, mainly in the growing season (Fig. 7b).

Precipitation

Overall, the precipitation amount and spatial variability in both simulations are higher than those in E-OBS throughout the year (Fig. 8). On one hand, the precipitation amount could be partly overestimated in REMO which is for example investigated in an earlier study by Kotlarski *et al*. (2005), who found an overestimation of precipitation in central Europe during winter. It is suggested that the overestimation of winter precipita-

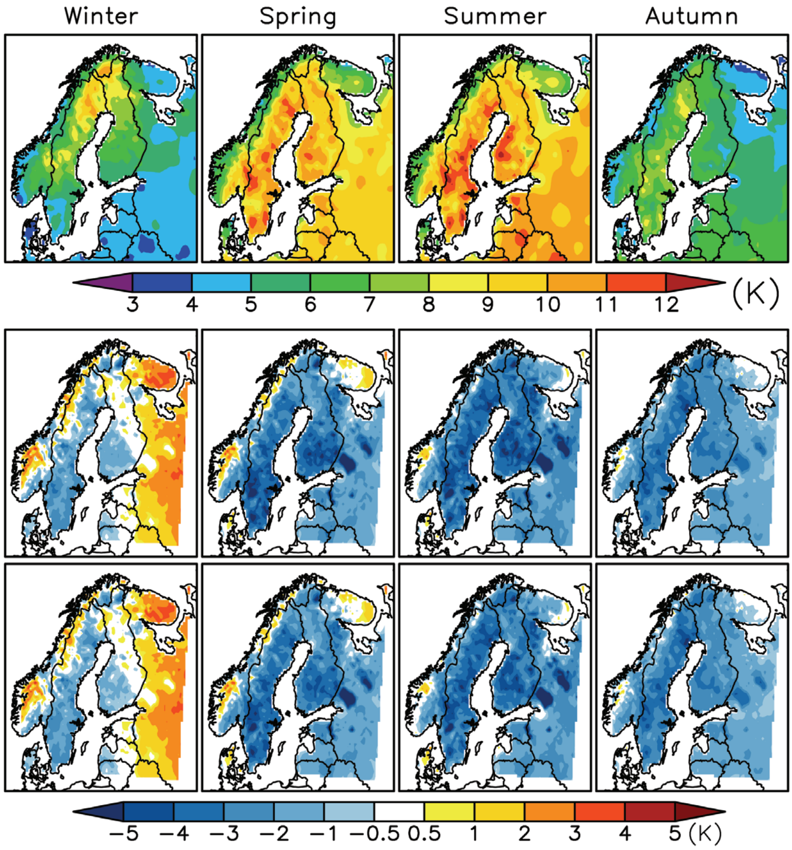

Fig. 6. Nine-year seasonal mean diurnal temperature ranges (K) in E-OBS (top), and the differences (REMO – E-OBS) in GLCCD simulation (middle) and in CLC simulation (bottom).

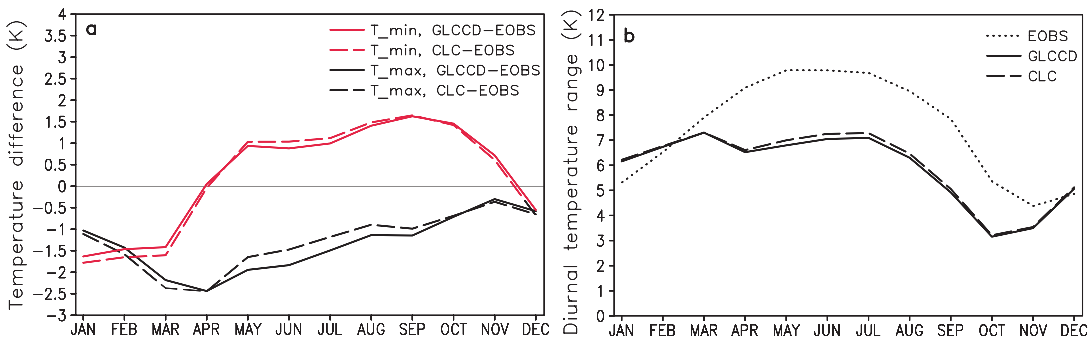

Fig. 7. (**a**) Area averaged monthly differences (REMO – E-OBS) for daily maximum 2-m air temperature (black) and daily minimum 2-m air temperature (red) in GLCCD (solid) simulation and in CLC simulation (dashed). (**b**) Area averaged monthly mean diurnal temperature ranges in GLCCD simulation (solid), in CLC simulation (dashed) and in E-OBS (dotted).

tion is strongly dependent on the boundary forcing (Jacob *et al*. 2007, Feldmann *et al*. 2008). On the other hand, it is well known that rain gauges often under-detect some precipitation, which is most problematic in regions and periods when snow takes up the main proportion of precipitation accompanied by high wind speeds (Frei *et al*. 2003). In particular, the amount of missing data from E-OBS precipitation stations has increased in recent years especially in winter. Although it is not suspected to be caused by snowfall disturbance because it is without any regional or eleva-

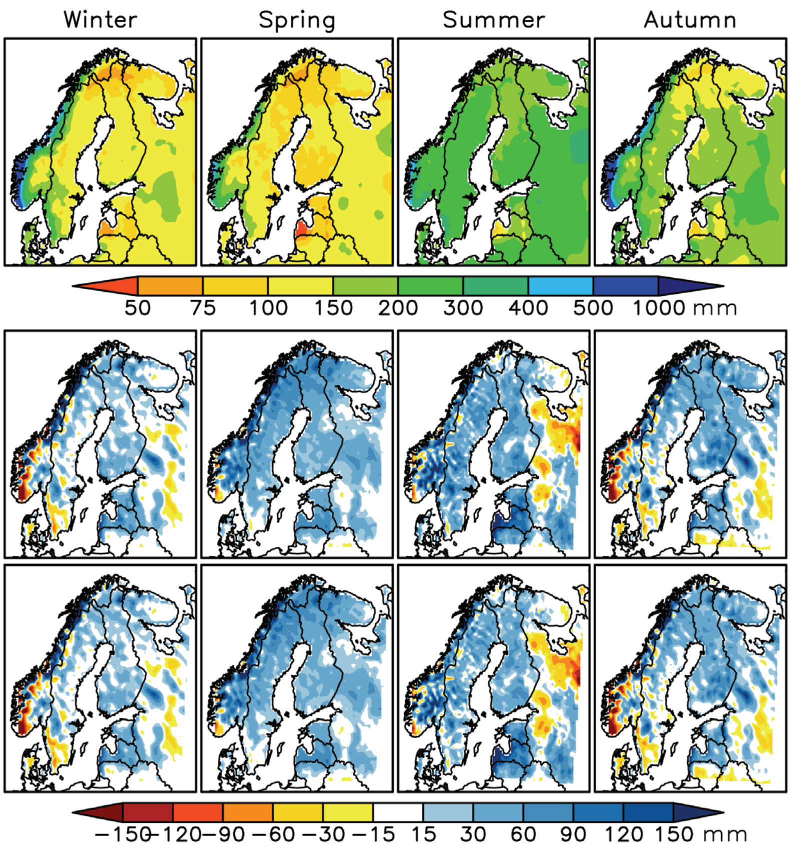

Fig. 8. Seasonal total precipitation (mm) in E-OBS (top), and the differences (REMO – E-OBS) in GLCCD simulation (middle) and in CLC simulation (bottom).

tional dependence, the uncertainty of E-OBS dataset is closely related to the number of stations and is generally larger at northern latitudes in winter due to a decreased spatial consistency (Haylock *et al*. 2008). The precipitation amount in northern Finland is lower than that in southern Finland in spring and summer in E-OBS, while such a spatial distribution does not exist in the REMO simulations. The reason for this may be that the density of precipitation stations is quite sparse in northern Finland. Besides, the very low precipitation in Latvia in E-OBS is most likely an artefact.

No remarkable differences in precipitation distribution between $GLCCD_{sim}$ and CLC_{sim} can be found (Fig. 8). However, areal averaged monthly total precipitation over land in CLC_{sim} is less than that in $GLCCD_{sim}$ throughout the year (Fig. 9). The biases of the monthly areal means of precipitation amount in CLC_{sim} over land relative to the E-OBS data are larger than 10 mm, except for the lowest overestimation which is roughly 9 mm in August. In addition, the reduction of the precipitation amount when the CLC-based surface library is used is more obvious in summer because regional land-atmosphere processes are more prevalent than the large-scale forcing during that time of the year.

Surface energy balance and hydrological cycle

Surface energy balance

To understand changes in the local surface temperature, we need to analyse the surface energy balance (Fig. 10). The change in net surface solar radiation is the dominant factor for the decreased surface temperature in dormancy season. Although the decreases in net surface solar radiation generally reach 10% in the study area in winter, changes in winter temperatures are not large (Fig. 5). It is because no differ-

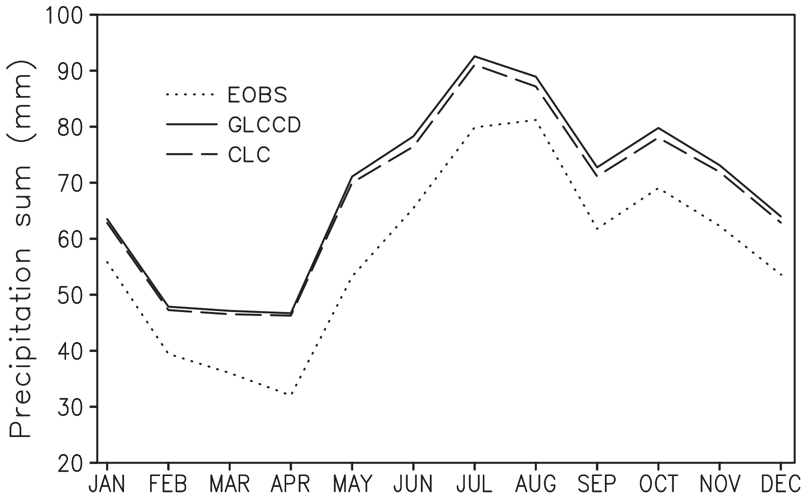

Fig. 9. Monthly mean precipitation amount averaged over all land grid points in GLCCD simulation (solid), in CLC simulation (dashed) and in E-OBS (dotted).

ences larger than ±2 W m^{-2} (not shown) can be found in net surface solar radiation between the two simulations due to the low incoming solar radiation in this high latitude domain in winter. The influences on surface albedo because of snow cover start from late-autumn and last until mid-spring in the study area (Fig. 11a). While the relatively large percentage changes in net surface solar radiation in winter are in line with the large percentage changes in surface albedo, the seasonal averaged percentage changes of net surface solar radiation in spring over the domain are smaller than ±4%. This can be attributed to the lower seasonal averaged total cloud cover (Fig. 11b) in spring which leads to more incoming solar radiation and also the already quite high net surface solar radiation in late spring.

ET starts to participate effectively in the energy balance as latent heat flux in mid-spring with the regrowth of vegetation. Less latent heat flux from mid-spring to mid-autumn in CLC_{sim} results in higher $T_{\text{max,2m}}$ as compared with that in $\text{GLCCD}_{\text{sim}}$ during this period (Fig. 7a). The total cloud cover also decreases in the growing season (Fig. 11b), which may be due to the reduced supply of moisture from ET (Göttel *et al.* 2008). The largest decreases happen in regions east of the Scandes during the snow-free period, because the mountain range serves as a natural obstacle weakening the influence of the large-scale atmospheric flow in the model's interior, and thus the regional-scale influences of vegetation predominate. In response to the lower total cloud cover, both the net surface solar radiation and the net surface thermal radiation increase in the growing season. The decreases in latent heat flux are roughly compensated by the increases in sensible heat flux in the growing season. In the seasonal means of autumn and winter, the heat transfer is directed from the atmosphere to the land surface because of a warmer atmosphere and a cooler land surface, thus the positive sign and decreases in the percentage changes of seasonal mean sensible heat fluxes can be interpreted as reduced downward heat conduction during these two seasons. In addition, we see smaller percentage changes in latent heat flux than in sensible heat flux in most areas of the domain, although the absolute changes in the two fluxes are almost equal, because latent heat fluxes are much larger than sensible heat fluxes in those areas.

In sum, the changes in energy fluxes lead to a simulated climate that is warmer and drier in the growing season and colder in the dormancy season in CLC_{sim}.

Hydrological cycle

The hydrological cycle is also important for understanding the temperature and precipitation differences between the two simulations (Fig. 12). As we already know from the discussion above, ET is the main driver of 2-m surface temperature in the growing season because it influences latent heat flux and cloud cover. The

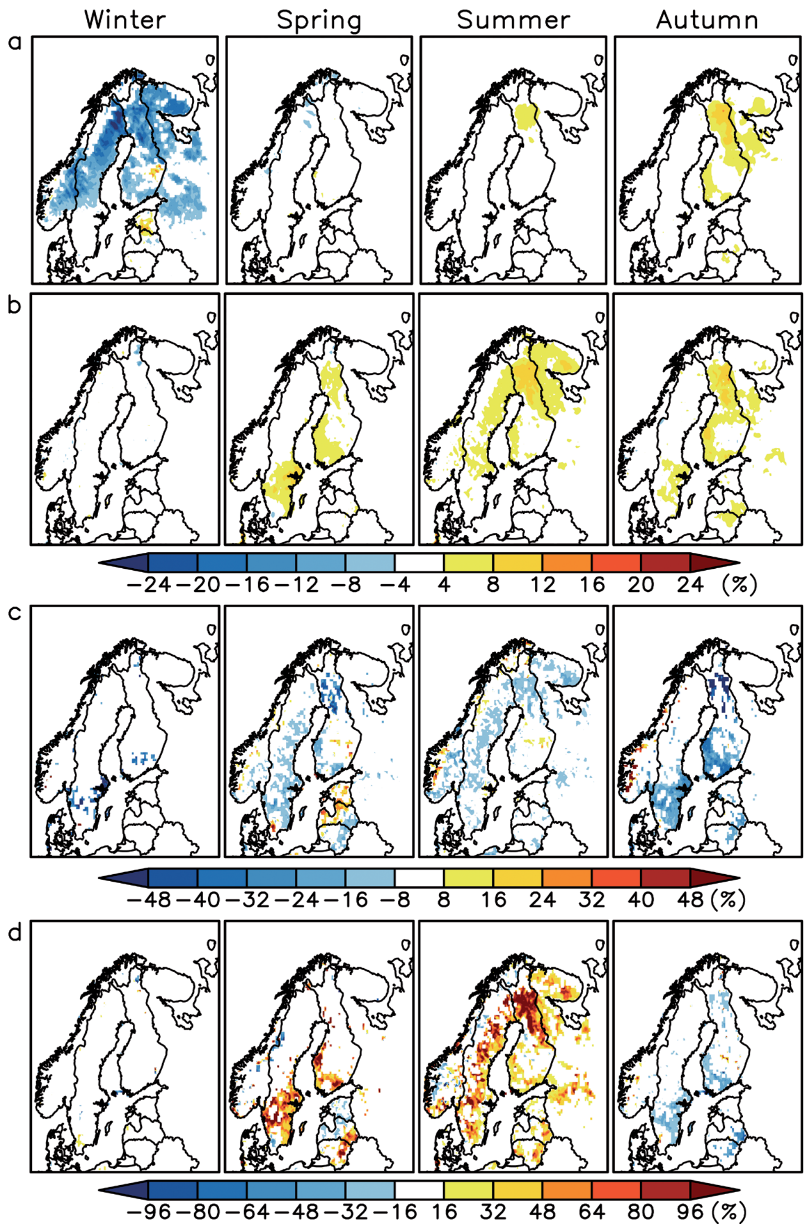

Fig. 10. Percentage changes [(CLC – GLCCD) × 100%/GLCCD] of seasonal mean surface energy fluxes between CLC simulation and GLCCD simulation. The panels from top to bottom are: (**a**) net surface solar radiation, (**b**) net surface thermal radiation, (**c**) latent heat flux, and (**d**) sensible heat flux. Note that the sign convention of energy fluxes in REMO is that the incoming solar radiation relative to the earth surface is assigned with a positive sign, whereas the outgoing surface thermal radiation, latent heat flux and sensible heat flux relative to the earth surface are assigned with negative signs.

other hydrological components (precipitation, soil wetness and total runoff) change either in accordance with or limit the changes in ET. One reason for the too cold $T_{max,2m}$ and too warm $T_{min,2m}$, as well as the overestimated precipitation in the two simulations in the growing season than those in E-OBS could be the simple bucket hydrology scheme in REMO, which cannot simulate a drying of the upper layer of the soil. Consequently, ET is relatively high when there is still water in the bucket which leads to a too high latent heat flux, a too high cloud cover and an accelerated hydrological cycle. In addition, a realistic simulation of cloud cover is acknowledged to still be a general challenge in regional climate modelling due to the high time variability of cloud cover and the uncertainties in the parameterization of clouds (Wyser *et al*. 2008).

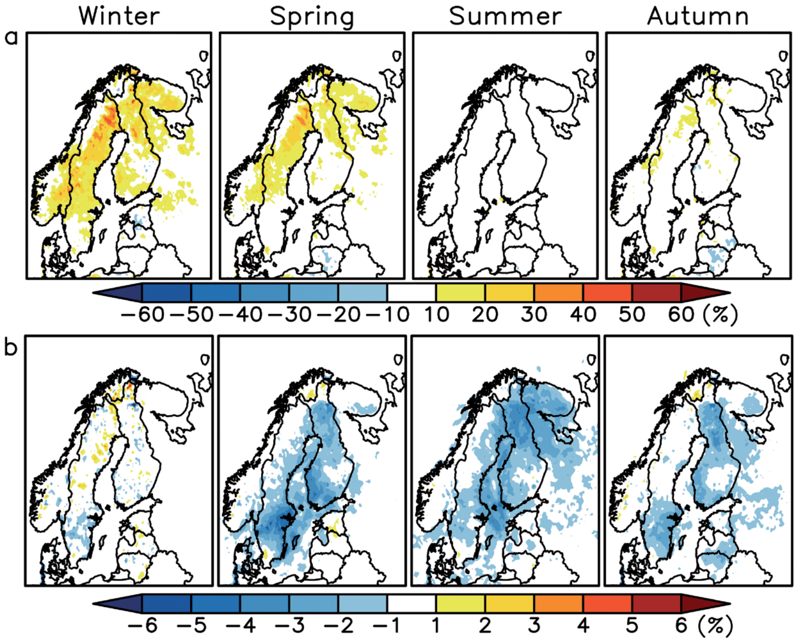

Fig. 11. Percentage changes [(CLC – GLCCD) × 100%/GLCCD] between CLC simulation and GLCCD simulation in: (**a**) seasonal mean surface albedo, and (**b**) seasonal mean total cloud cover.

Comparing the hydrological cycle in the two simulations (Fig. 12), the reduction in ET due to the decreased LAI and vegetation fractional cover, which outweighs the decreases in precipitation in CLC_{sim}, leads to an increased moisture divergence, especially in the growing season. As a result, the total runoff and soil wetness increase over most land areas in the domain except in the Scandes which is influenced by decreased field capacity (Fig. 3c). The percentage changes of ET in winter are quite high, more than ±50%, in many parts of the domain but the changes are actually smaller than 14 mm in 3 months (not shown), whereas the percentage changes in ET in summer are smaller compared to those in other seasons which are only due to the large ET in summer. The changes in the ET in winter are suspected to be affected by the smaller inland water fraction in CLC which leads to less heat and moisture to be released to the atmosphere from lakes, especially in the period when the environment is cool but lakes are still not frozen. The geographical patterns of precipitation changes are more or less in response to the changes in ET in winter, spring and autumn, but rather chaotic in summer due to the strong land-atmosphere interactions during this time.

Summary and conclusion

In this study, the land cover description of REMO was improved in the northern European domain by implementing the 100-m-resolution CLC derived in 2006. This replaces the standard 1-km-resolution GLCCD that dates back to the early 1990s. In this work, REMO is driven by ERA-Interim reanalysis data and is applied to simulate the present-day climate for the years from 2001 to 2009 by using both CLC and GLCCD. Therefore, differences in the results of the two simulations arise from the different land cover distributions and from the readjustment of parameter values for Conifer Boreal Forest. The intention of this work was to set up a more realistic reference for future land cover change studies by using the updated present-day land cover map and to gain more insight into the performance of REMO in climate simulations in a high-latitude domain.

Comparing the results from CLC_{sim} with those from the reference run employing GLCCD, the monthly areal mean DTR is slightly increased in the growing season despite the fact that both REMO simulations still underestimate the range by about 2 to 3 K in comparison with

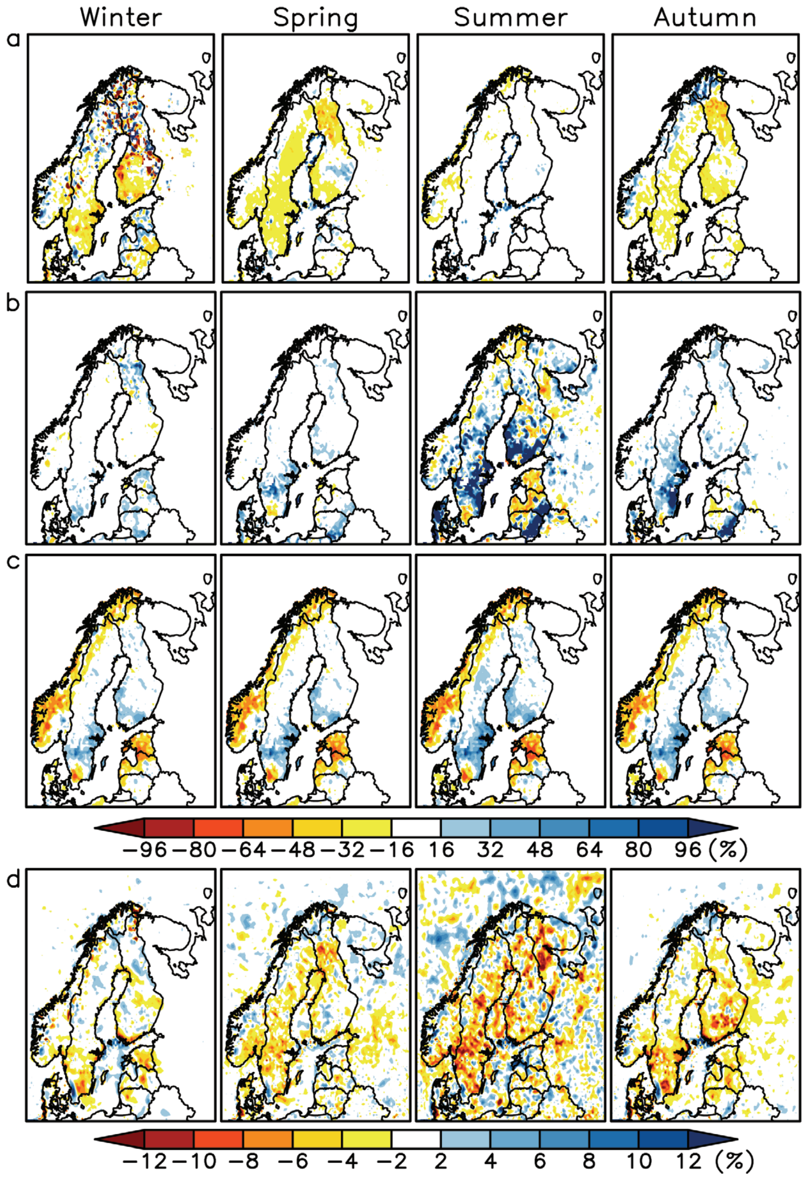

Fig. 12. Percentage changes [(CLC – GLCCD) × 100%/GLCCD] of seasonal total of hydrological components between CLC simulation and GLCCD simulation. The panels from top to bottom are: (**a**) evapotranspiration, (**b**) total runoff, (**c**) soil wetness, and (**d**) precipitation. Note that only the water which is transported from land to atmosphere, i.e. evapotranspiration, has a negative sign.

the E-OBS observation data. The overestimation of the annual areal mean precipitation over land of about 27% in GLCCD$_{sim}$ is slightly reduced in CLC$_{sim}$. Locally, the changes at a few grid points are much stronger for precipitation and temperature due to the local land cover changes. Changes in the simulated energy balance and hydrological cycle can be helpful in understanding the changes in the 2-m air temperature and precipitation. In conclusion, surface albedo and ET are the dominating factors during snow cover period and during growing season, respectively, for the differences in near-surface temperature between CLC$_{sim}$ and GLCCD$_{sim}$. The decreased ET also causes a reduction in precipitation.

The deviations between the simulation results by REMO and E-OBS in 2-m air temperature and precipitation are considered to stem from uncertainties in both REMO simulations as well as in E-OBS. The areal averaged $T_{max,2m}$ in the REMO simulations are lower than those in E-OBS throughout the year, whereas the areal averaged $T_{\text{min,2m}}$ in the REMO simulations are higher than those in E-OBS in the growing season but lower in the dormancy season. Overall, the underestimated nighttime cooling and daytime warming effects lead to a reduction in the DTR in both REMO simulations. Besides, throughout the year REMO simulates higher precipitation amounts than observed.

The reasons for the deviations between REMO simulation results and E-OBS are manifold. The translations between the vegetation types in CLC and GLCCD presented in this study include uncertainties. Further efforts can be made to improve the parameter values in the land surface scheme of REMO with the aim of giving a better description of the physiological characteristics of vegetation, especially in the northern European domain. Also, the influence from boundary forcing data should not be neglected because the domain is relatively small which means less freedom for REMO. Moreover, model physics and parameterizations can be considered a more important source of uncertainty. Further model developments with the implementation of a lake model (J. Kaurola, Finnish Meteorological Institute, pers. comm.) and a 5-layer soil hydrology scheme (S. Hagemann, MPI for Meteorology, pers. comm.) are undergoing. These developments will make REMO become more realistic in the physical sense and should diminish the deviations from observations in model simulations to some extent. In addition, the uncertainties in E-OBS due to a relatively sparse measurement station density in northern Europe, measurement errors and imperfect interpolation methods should also be considered in the analysis of deviations (Haylock *et al*. 2008).

Overall, improvements in the REMO simulation for present-day climate in a high-latitude domain that covers Fennoscandian countries are achieved by using high-resolution CLC. Significant model improvements cannot, however, be obtained when merely changing the land cover description in a realistic way. In the near future, a historic land cover map traced back to the 1920s with no wetland forestation and future land cover maps based on projected forest management strategies in Finland will be introduced into REMO to study the regional climate effects in a Fennoscandian domain. However, because the main focuses are the differences between the climate simulations based on present, past and future land cover conditions, the results obtained when employing CLC can be regarded as a valuable reference.

Acknowledgements: This study was partly funded by Helsinki University Centre for Environment (HENVI). We also acknowledge the E-OBS dataset from the EU-FP6 project ENSEMBLES (http://ensembles-eu.metoffice.com) and the data providers in the ECA&D project (http://www.ecad.eu). The authors would like to thank Diana Rechid and Stefan Hagemann from Max Planck Institute for Meteorology, Hamburg, for kindly providing answers to many questions concerning REMO and its land surface scheme. We also appreciate Tuula Aalto for her help. Special thanks to Declan O' Donnell for grammar checking.

References

Aldrian E., Dümenil-Gates L., Jacob D., Podzun R. & Gunawan D. 2004. Long-term simulation of Indonesian rainfall with the MPI regional model. *Clim. Dynam.* 22: 795–814.

Bala G., Caldeira K., Wickett M., Phillips T.J., Lobell D.B., Delire C. & Mirin A. 2007. Combined climate and carbon-cycle effects of large-scale deforestation. *P. Natl. Acad. Sci. USA* 104(16): 6550–6555.

Bathiany S., Claussen M., Brovkin V., Raddatz T. & Gayler V. 2010. Combined biogeophysical and biogeochemical effects of large-scale forest cover changes in the MPI earth system model. *Biogeosciences* 7: 1383–1399.

Betts R.A. 2001. Biogeophysical impacts of land use on present-day climate: Near-surface temperature change and radiative forcing. *Atmos. Sci. Lett.* 2: 39–51.

Betts A.K. & Ball J.H. 1997. Albedo over the boreal forest. *J. Geophys. Res.* 102: 28901–28910.

Cheng F.Y. & Byun D.W. 2008. Application of high resolution land use and land cover data for atmospheric modeling in the Houston-Galveston metropolitan area, Part I: Meteorological simulation results. *Atmos. Environ.* 42: 7795–7811.

Claussen M., Lohmann U., Roeckner E. & Schulzweida U. 1994. *A global dataset of land surface parameters*. MPI Report No. 135, Max Planck Institute for Meteorology, Hamburg.

Davies H.C. 1976. A lateral boundary formulation for multi-level prediction models. *Q. J. R. Meteorol. Soc.* 102: 405–418.

Dümenil L. & Todini E. 1992. A rainfall-runoff scheme for use in the Hamburg climate model. In: O'Kane J.P. (ed.), *Advances in theoretical hydrology: a tribune to James Dooge*, Elsevier,Amsterdam, pp. 129–157.

European Environment Agency 2007. *CLC2006 technical guidelines*. EEA Technical Report No. 17, Copenhagen, available at http://www.eea.europa.eu/publications/technical_report_2007_17/at_download/file.

FAO/UNESCO 1971–1981. *Soil map of the world*. FAO/UNESCO, Paris.

Feldmann H., Fruh B., Schadler G., Panitz H.J., Keuler K., Jacob D. & Lorenz P. 2008. Evaluation of the precipitation for south-western Germany from high resolution simulations with regional climate models. *Meteorol. Z.* 17: 455–465.

Frei C., Christensen J.H., Déqué M., Jacob D., Jones R.G., & Vidale, P.L. 2003. Daily precipitation statistics in regional climate models: Evaluation and intercomparison for the European Alps. *J. Geophys. Res.* 108(D3), 4124, doi:10.1029/2002JD002287.

Gálos B., Mátyás C. & Jacob D. 2011. Regional characteristics of climate change altering effects of afforestation. *Environ. Res. Lett.* 6: 044010, doi. 10.1088/1748-9326/6/4/044010.

Göttel H., Alexander J., Keup-Thiel E., Rechid D., Hagemann S., Blome T., Wolf A. & Jacob D. 2008. Influence of changed vegetations fields on regional climate simulations in the Barents Sea Region. *Climatic Change* 87: 35–50.

Hagemann S. 2002. *An improved land surface parameter data set for global and regional climate models*. MPI Report No. 336, Max Planck Institute for Meteorology, Hamburg. [Available at http://www.researchgate.net/publication/27269130_An_Improved_Land_Surface_Parameter_Dataset_for_Global_and_Regional_Climate_Models/file/79e41505c535bce979.pdf].

Hagemann S. & Gates L.D. 2003. Improving a subgrid runoff parameterization scheme for climate models by the use of high resolution data derived from satellite observations. *Clim. Dynam.* 21: 349–359.

Hagemann S., Botzet M., Dümenil L. & Machenhauer B. 1999. *Derivation of global GCM boundary conditions from 1 km land use satellite data*. MPI Report No. 289, Max Planck Institute for Meteorology, Hamburg. [Available at http://www.mpimet.mpg.de/fileadmin/publikationen/Reports/max_scirep_289.pdf].

Haylock M.R., Hofstra N., Klein Tank A.M.G., Klok E.J., Jones P.D. & New M. 2008. A European daily high-resolution gridded data set of surface temperature and precipitation for 1950–2006. *J. Geophys. Res.* 113, D20119, doi:10.1029/2008JD010201.

Jacob D. 2001. A note to the simulation of the annual and inter-annual variability of the water budget over the Baltic Sea drainage basin. *Meteorol. Atmos. Phys.* 77: 61–73.

Jacob D. & Podzun R. 1997. Sensitivity studies with the regional climate model REMO. *Meteorol. Atmos. Phys.* 63: 119–129.

Jacob D., Van den Hurk B.J.J.M., Andrae U., Elgered G., Fortelius C., Graham L.P., Jackson S.D., Karstens U., Köpken Chr., Lindau R., Podzun R., Rockel B., Rubel F., Sass B.H., Smith R.N.B. & Yang X. 2001. A comprehensive model inter-comparison study investigating the water budget during the BALTEX-PIDCAP period. *Meteorol. Atmos. Phys.* 7: 19–43.

Jacob D., Bärring L., Christensen O.B., Christensen J.H., de Castro M., Déqué M., Giorgi, F., Hagemann S., Hirschi M., Jones R., Kjellström E. Lenderink G., Rockel B., Sánchez E., Schär C., Seneviratne S.I., Somot S., Van Ulden A. & Van den Hurk B. 2007. An inter-comparison of regional climate models for Europe: model performance in present-day climate. *Climatic Change* 81: 31–52.

Kotlarski S. 2007. *A subgrid glacier parameterisation for use in regional climate modelling*. Ph.D. thesis, University of Hamburg, Max Planck Institute for Meteorology, Reports on Earth System Science No. 42, Hamburg. [Available at http://www.mpimet.mpg.de/fileadmin/publikationen/Reports/WEB_BzE_42.pdf].

Kotlarski S., Block A., Böhm U., Jacob D., Keuler K., Knoche R., Rechid D. & Walter A. 2005. Regional climate model simulations as input for hydrological applications: evaluation of uncertainties. *Adv. Geosci.* 5: 119–125.

Legates D.R. & Willmott C.J. 1990. Mean seasonal and spatial variability in global surface air temperature. *Theor. Appl. Climatol.* 41: 11–21.

Lohila A., Minkkinen K., Laine J., Savolainen I., Tuovinen J.-P., Korhonen L., Laurila T., Tietäväinen H. & Laaksonen A. 2010. Forestation of boreal peatlands — impacts of changing albedo and greenhouse gas fluxes on radiative forcing. *J. Geophys. Res. (Biogeosciences)* 115, G04011, doi:10.1029/2010JG001327.

Loveland T.R., Reed B.C., Brown J.F., Ohlen D.O., Zhu Z., Yang L. & Merchant J.W. 2000. Development of a global land cover characteristics database and IGBP DISCover from 1 km AVHRR data. *Int. J. Remote Sens.* 21: 1303–1330.

Majewski D. 1991. The Europa-Modell of the Deutscher Wetterdienst. *ECMWF Seminar on Numerical Methods in Atmospheric Models* 2: 147–191.

Mason P.J. 1988. The formation of areally-averaged roughness lengths. *Q. J. R. Meteorol. Soc.* 114: 399–420.

Nobre C.A., Dias M.A.S., Culf A.D., Polcher J., Gash J.H., Marengo J.A. & Avissar R. 2004. The Amazonian climate. In: Kabat P., Claussen M., Dirmeyer P.A., Gash J.H.C., De Guenni L.B., Meybeck M., Pielke R., Vörösmarty C.I., Hutjes R.W.A. & Lütkemeier S. (eds.), *Vegetation, water, humans and the climate: a new perspective on an interactive system*, Springer, Berlin, Heidelberg, pp. 79–92.

Olson J.S. 1994a. *Global ecosystem framework 1*. Definitions, EROS Data Center Internal Report, Sioux Falls, SD, USA.

Olson J.S. 1994b. *Global ecosystem framework 2*. Translation strategy, EROS Data Center Internal Report, Sioux Falls, SD, USA.

Pielke R.A., Avissar R., Raupach M., Dolman A.J., Zeng X. & Denning A.S. 1998. Interactions between the atmosphere and terrestrial ecosystems: influence on weather and climate. *Glob. Change Biol.* 4: 461–475.

Pietikäinen J.-P., O'Donnell D., Teichmann C., Karstens U., Pfeifer S., Kazil J., Podzun R., Fiedler S., Kokkola H., Birmili W., O'Dowd C., Baltensperger U., Weingartner E., Gehrig R., Spindler G., Kulmala M., Feichter J., Jacob D. & Laaksonen A. 2012. The regional aerosol-climate model REMO-HAM. *Geosci. Model Dev.* 5:

1323–1339.

Pitman A.J., Dolman H., Kruijt B., Valentini R. & Baldocchi D. 2004. The climate near the ground. In: Kabat P., Claussen M., Dirmeyer P.A., Gash J.H.C., De Guenni L.B., Meybeck M., Pielke R., Vörösmarty C.I., Hutjes R.W.A. & Lütkemeier S. (eds.), *Vegetation, water, humans and the climate: a new perspective on an interactive system*, Springer, Berlin, Heidelberg, pp. 9–19.

Preuschmann S. 2012. *Regional surface albedo characteristics — analysis of albedo data and application to land-cover changes for a regional climate model*. Ph.D. thesis, University of Hamburg, Max Planck Institute for Meteorology, Reports on Earth System Science, No. 117, Hamburg. [Available at http://www.mpimet.mpg.de/fileadmin/publikationen/Reports/WEB_BzE_117.pdf].

Rechid D. 2008. *On biogeophysical interactions between vegetation phenology and climate simulated over Europe*. Ph.D. thesis, University of Hamburg, Max Planck Institute for Meteorology, Reports on Earth System Science, No. 61, Hamburg. [Available at http://www.mpimet.mpg.de/fileadmin/publikationen/Reports/WEB_BzE_61.pdf].

Rechid D. 2009. *Land surface scheme of REMO*. Internal report, Max Planck Institute for Meteorology, Hamburg. [Available at http://www.remo-rcm.de/fileadmin/user upload/remo/UBA/pdf/LandSurfaceScheme REMO short-summary.pdf].

Rechid D., Raddatz T.J. & Jacob D. 2009. Parameterization of snow-free land surface albedo as a function of vegetation phenology based on MODIS data and applied in climate modelling. *Theor. Appl. Climatol.* 95: 245–255.

Roeckner E., Arpe K., Bengtsson L., Christoph M., Claussen M., Dümenil L., Esch M., Giorgetta M., Schlese U. & Schulzweida U. 1996. *The atmospheric general circulation model ECHAM-4: Model description and simulation of present-day climate*. MPI Report No. 218. Max Planck Institute for Meteorology, Hamburg. [Available at http://www.mpimet.mpg.de/fileadmin/publikationen/Reports/MPI-Report_218.pdf].

Sertel E., Robock A. & Ormeci C. 2010. Impacts of land cover data quality on regional climate simulations. *Int. J. Climatol.* 30: 1942–1953.

Semmler T. 2002. *Der Wasser- und Energiehaushalt der arktischen Atmosphäre*. Ph.D. thesis, University of Hamburg, Max-Planck-Institut für Meteorologie, Hamburg. [Available at http://www.mpimet.mpg.de/fileadmin/publikationen/Ex85.pdf].

Semmler T., Jacob D., Schlünzen K.H. & Podzun R. 2004. Influence of sea ice treatment in a regional climate model on boundary layer values in the Fram Strait region. *Mon. Weather Rev.* 132: 985–999.

Simmons A., Uppala S., Dee D. & Kobayashi S. 2007. *ERA-Interim: New ECMWF reanalysis products from 1989 onwards*. ECMWF newsletter No. 110: 25–35.

Solantie R. 1994. *Suurten suo-ojitusten vaikutus ilman lämpötilaan erityisesti Alajärven Möksyn havaintojen perusteella* [*The impact of large scale wetland drainage on air temperature based on observations in Möksyn and Alajärven*]. Meteorol. publications 29, Finnish Meteorological Institute, Helsinki. [In Finnish with English summary].

Sud Y.C., Lau W.K., Walker G.K., Kim J.H., Liston G.E. & Sellers P.J. 1996. Biogeophysical consequences of a tropical deforestation scenario: a GCM simulation study. *J. Climate* 9: 3225–3247.

Tibaldi S. & Geleyn J.F. 1981. *The production of a new orography, land-sea mask and associated climatological surface fields for operational purposes*. ECMWF Technical Memorandum No. 40, ECMWF, Reading, United Kingdom.

U.S. Geological Survey 2001. *Global land cover characteristics data base version 2.0*. U.S. Geological Survey. [Available at http://edc2.usgs.gov/glcc/glcc.php].

Venäläinen A., Rontu L. & Solantie R. 1999. On the influence of peatland draining on local climate. *Boreal Env. Res.* 4: 89–100.

Wyser K., Jones C.G., Du P., Girard E., Willén U., Cassano J., Christensen J.H., Curry J.A., Dethloff K., Haugen J.-E., Jacob D., Koltzow M., Laprise R., Lynch A., Pfeifer S., Rinke A., Serreze M., Shaw M.J., Tjernstrom M. & Zagar M. 2008. An evaluation of Arctic cloud and radiation processes during the SHEBA year: simulation results from eight Arctic regional climate models. *Clim. Dynam.* 30: 203–223.

Yucel I. 2006. Effects of implementing MODIS land cover and albedo in MM5 at two contrasting US regions. *J. Hydrometeorol.* 7: 1043–1060.

Zobler L. 1986. *A world soil file for global climate modelling*. NASA Technical Memorandum 87802, NASA Goddard Institute for Space Studies, New York, U.S.A.